Carbohydrate Polymers 106 (2014) 305–311

Contents lists available at ScienceDirect

Carbohydrate Polymers

journal homepage: www.elsevier.com/locate/carbpol

Thermal and electrical properties of starch–graphene oxide nanocomposites improved by photochemical treatment

Priscilla P. Peregrino[a], Maria J.A. Sales[a], Mauro F.P. da Silva[b], Maria A.G. Soler[c], Luiz F.L. da Silva[d], Sanclayton G.C. Moreira[d], Leonardo G. Paterno[a,*]

[a] Universidade de Brasília, Instituto de Química, Brasília, DF 70910-900, Brazil
[b] Pontifícia Universidade Católica de São Paulo, FCET, São Paulo, SP 01303-050, Brazil
[c] Universidade de Brasília, Instituto de Física, Brasília, DF 70910-900, Brazil
[d] Universidade Federal do Pará, Instituto de Ciências, Exatas e Naturais (ICEN), Belém, PA 66075-900, Brazil

ARTICLE INFO

Article history:
Received 11 January 2014
Received in revised form 1 February 2014
Accepted 3 February 2014
Available online 9 February 2014

Keywords:
Bionanocomposites
Starch
Graphene oxide
Thermal properties
Electrical properties
Photochemical reduction

ABSTRACT

Bionanocomposite films have been prepared by casting an aqueous suspension of acetylated starch (ST) and poly(vinyl alcohol) (PVA) loaded with graphene oxide (GO). A photochemical and reagentless method has been successfully performed to convert the GO phase into reduced graphene oxide (RGO). The nanocomposites have displayed improved thermal and electrical properties when the amount of the GO phase is increased and properly converted to RGO. The molecular-level interactions between components are mainly hydrogen-bonding type according to attenuated total reflectance-Fourier transform infrared (ATR-FTIR) and Raman spectroscopies, as well as thermogravimetric analysis (TGA). Scanning electron microscopy (SEM) has confirmed the effective mixing between the GO and the ST–PVA matrix. The thermal diffusivity and electrical resistivity of ST–GO nanocomposites have increased one order and decreased two orders of magnitude, respectively, after the photochemical treatment. These findings have confirmed the effectiveness of the proposed approach to produce starch-based nanocomposites with improved thermal and electrical properties.

1. Introduction

Bionanocomposites today, represent an environmentally friendly strategy for the production of novel materials while employing raw components from the plenty source provided by biomass. These systems are comprised by a continuous biopolymer matrix loaded with nanofillers, usually inorganic in nature. While the biopolymer matrix ensures the material's biodegradability, nanofillers provide the required thermal, mechanical, and electrical properties, usually very poor in the biopolymer alone (Darder, Aranda, & Ruiz-Hitzky, 2007).

Among several biopolymers for bionanocomposites, starch is very appealing because of its low cost and availability from different natural sources such as vegetables and cereals (Paraginski et al., 2014). Besides the nourishing value, the film forming ability has given to starch a more remarkable role, for example, in food packaging. Starch-based films are biodegradable and edible and therefore, are potential substitutes for many synthetic packaging materials and pose negligible harm to the environment (Tang, Kumar, Alavi, & Sandeep, 2012).

On the other hand, starch exhibits poor thermal and electrical properties, which restrict its widespread use. This apparent limitation can be, however, circumvented by adding nanofillers such as graphene oxide (GO) sheets. GO can be considered a precursor for the preparation of graphene-based materials (Zhu et al., 2010). Besides that, GO is highly hydrophilic and dispersible in water, features that readily enable mixing and compatibility of GO and starch, as well as with other polymeric matrixes (Jaber-Ansari & Hersam, 2012). In fact, this possibility has been recently verified by different research groups. For example, Li et al. (Li, Liu, & Ma, 2011) and Ma et al. (Ma, Liu, Li, & Wang, 2012) have carried out a pioneer research on nanocomposites made of starch and GO when they found that GO increases the Young modulus and the thermal stability of pure starch. A subsequent investigation has been conducted by He and colleagues (He et al., 2013) when they observed that GO prevents starch from degradation in both acidic and alkaline environments. Rodríguez-González et al. (2012) have observed that the mechanical properties (storage modulus) of a chitosan–starch matrix is substantially improved (about 900%) with only 0.5 wt% of GO. Ashori's group have introduced the

* Corresponding author. Tel.: +55 61 3107 3869; fax: +55 61 3107 3900.
E-mail address: lpaterno@unb.br (L.G. Paterno).

http://dx.doi.org/10.1016/j.carbpol.2014.02.008
0144-8617/

melting processing of polypropylene composites with either sugar cane bagasse or wood flours, both enriched with graphene nanoplatelets (Sheshmani, Ashori, & Fashapoyeh, 2013; Chaharmahali, Hamzeh, Ebrahimi, Ashori, & Ghasemi, 2014). They have observed that there is an optimum graphene content for the bionanocomposites to reaching the best mechanical properties.

However, another main interest on introducing GO into common polymeric matrices is to provide or enhance their optoelectronic properties. GO is usually obtained after chemical exfoliation of graphite which is a more affordable and readily available carbon source (Jaber-Ansari & Hersam, 2012). GO resembles graphene by its monoatomic dimension, but it also differs significantly from it because of oxygen bearing functionalities such as hydroxyl, carbonyl, carboxyl, and epoxy. These functionalities disrupt part of the sp^2 conjugation and turn GO into an electrical insulating material. However, part of optical, electronic and many other properties of pristine graphene can be restored after proper reduction of GO (Stankovich et al., 2007; Tung, Allen, Yang, & Kaner, 2009). Concerning that, we have produced starch-based nanocomposite films in which GO is introduced and photochemically converted into its reduced form, namely reduced graphene oxide (RGO). The reduced nanocomposite has thermal and electrical properties improved after the photochemical process, which is easy to perform and does not demand for hazardous chemicals such as hydrazine or sodium borohydride.

Herein, we describe the preparation and investigate the properties of bionanocomposite cast films made of starch filled with GO sheets (ST–GO). UV–vis, attenuated total reflectance-Fourier transform infrared (ATR-FTIR) and Raman spectroscopies are employed to determine the structure and infer about the molecular-level interaction between the starch matrix and GO sheets. An additional study performed with thermogravimetric analysis (TGA) provides further evidence for the interaction of bionanocomposites' components. In order to restore part of the outstanding properties of graphene, we have submitted the bionanocomposite films to UV radiation (254 nm). After a proper irradiation time, the thermal diffusivity and electrical properties of ST–GO films are significantly improved, due to partial reduction of GO, as confirmed by Raman and UV–vis spectroscopies.

2. Experimental

2.1. Materials

Graphite powder (Union Carbide, SP-1 grade, 100 μm), acetylated starch (Avebe Guaíra Amidos, Brazil), poly(vinyl alcohol)-PVA (Sigma–Aldrich, 89,000–98,000 g mol^{-1}), H_2SO_4 98%, HNO_3 67%, $KClO_3$, $KHCO_3$, HCl 37%, NH_4OH 47%, were purchased from Sigma–Aldrich, Merck and Carlo Erba, all analytical grade or better and used as received. Ultrapure water (18.2 MΩ cm) purified by a Milli-Pore Milli-Q system was used throughout all procedures. Graphene oxide (GO) was obtained via a two step procedure. In the first, graphite powder was oxidized in a mixture of 1:2 H_2SO_4/HNO_3 (2:1 v/v) and $KClO_3$ as originally described by Staudenmaier (1898) with some modification as described elsewhere (Silva, Costa, Triboni, Politi, & Isolani, 2010). In the second step, the as-obtained graphitic oxide was suspended in NH_4OH aqueous solution (pH 10) under sonication (150 W, 1 h). The resulting GO suspension was centrifuged at 15,000 rpm for 20 min to remove remaining solids and stored for the nanocomposites' preparation.

2.2. Preparation of starch–GO (ST–GO) nanocomposites.

5 g of acetylated starch (ST) and 0.15 g of PVA were suspended together in 40 mL of deionized water. PVA was used as an additional plasticizer (besides water) for starch. The milky ST-PVA suspension was kept under magnetic stirring at 90 °C for 1 h in order to gelatinize starch and ensure their complete mixing. In another vessel, additional 0.05 g of PVA were dissolved in deionized water (70 °C) under magnetic stirring until reaching its complete dissolution. A fixed volume of the GO aqueous suspension was then added to this PVA solution under magnetic stirring at 70 °C until a homogenous solution was obtained. This procedure was adopted to enhance compatibility between GO and starch and to avoid GO flocculation. Four different PVA–GO solutions with different GO concentrations were prepared. A fifth PVA solution absent of GO was prepared and used for the preparation of the control film. For the preparation of ST–GO nanocomposite films, the PVA–GO solution was added slowly to the ST–PVA suspension under magnetic stirring at 60 °C. The stirring and temperature were maintained for more than 1 h after addition of the PVA–GO solution. The resulting pale yellow suspension was then cast onto Petri dishes (diameter: 10 cm) and left drying in oven (60 °C) for 24 h. The control film (absent of GO) was prepared under the same procedure. Five nanocomposite samples were prepared, labeled as: ST-C (control), ST–GO-010, ST–GO-025, ST–GO-050, and ST–GO-075. The numbers refer to the weight percentage of GO in the nanocomposite (regarding the starch mass).

2.3. UV treatment of ST–GO samples

In order to induce the photochemical reduction of GO, ST–GO samples (1.0 × 2.5 cm^2) were exposed to UV light (254 nm) (Boitton Instrumentos, Brazil) for different periods of time up to 2 h. UV–vis spectra of films were obtained after different irradiation time to monitor the photochemical effect. For comparison, the control film (absent of GO) underwent the same treatment and monitoring. The ATR-FTIR and Raman spectra, thermal diffusivity, and current *versus* potential curves of un- and treated samples were measured in order to evaluate the effectiveness of the photochemical treatment.

2.4. Film characterizations

The chemical structure of nanocomposite films was assessed by UV–vis (Varian Cary 5000), ATR-FTIR (Varian 640IR) and Raman (Jobin Yvon T 6400, 514 nm laser line, 0.3 mW) spectroscopies.

Film's morphology (surface and cross-section areas) was evaluated by scanning electron microscope (JEOL 440A). Film's cross-section was made after submitting films to liquid nitrogen and further cracking. Samples were attached to brass stubs with the aid of conductive carbon tape and gold-coated by sputtering.

Thermogravimetry (TGA) and derivative thermogravimetry (DTG) analysis were conducted in a DTG-60H Shimadzu thermoanalyzer. Powdered samples (~5 mg) were filled in platinum pans and evaluated under nitrogen atmosphere (30 mL min^{-1}), at heating rate of 10 °C min^{-1}.

The thermal diffusivity of film samples was determined by photopyroelectric spectroscopy (PPS) as described by Mandelis and Zver (1985), with the aid of a home-made experimental setup. The PPS working principle bases on the irradiation of a solid sample with a monochromatic source and measurement of that part of optical energy that is converted into heat by non-radiative deexcitation processes within the solid. According to the model described by Mandelis and Zver, a non-uniform variation on temperature leads to a voltage drop in the pyroelectric transductor. The voltage drop is related to the sample's thermal diffusivity, according to Eq. (1) as follows:

$$V(\omega) = A\left[\frac{\eta_s \alpha_s}{k_p(1+b_{sp})\omega}\right]\exp\left[-\left(\frac{\omega}{2\alpha_s}\right)^{1/2} L_s\right] \quad (1)$$

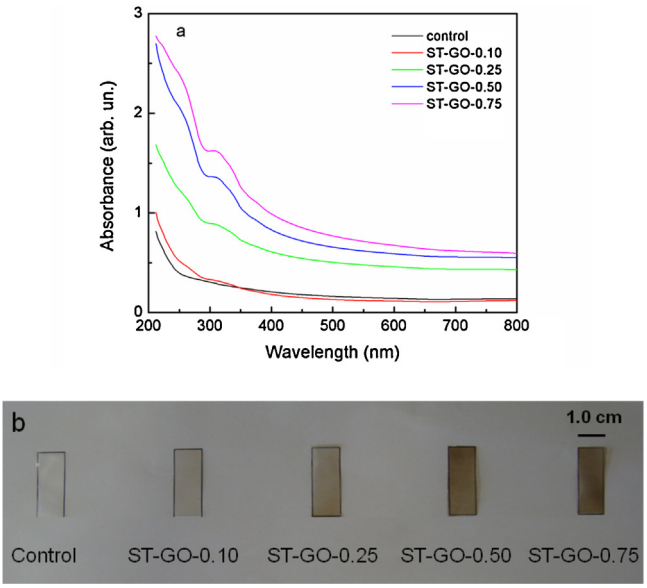

Fig. 1. UV–vis absorption spectra (a) and digital snapshots (b) of ST–GO nanocomposites with different GO loadings (in weight percentage), as indicated. (For interpretation of the references to colour in this figure legend, the reader is referred to the web version of this article.)

where η_s is the sample's nonradiative conversion efficiency; α_p and α_s are the thermal diffusivity of the pyroelectric transducer and sample, respectively; k_p is the transducer's thermal conductivity; b_{sp} is the ratio between the product of sample's and transducer's thermal conductivity and diffusivity ($=k_s\alpha_s/k_p\alpha_p$); ω is the angular frequency of the electrical field; and L_s is the sample's thickness. In addition, the parameter A ($=pI_0/2k\epsilon_0$), where p is the pyroelectric coefficient of the transducer, I_0 is the incident light source irradiance, k is the transducer's dielectric constant, and ϵ_0 is the vacuum permittivity ($=8.854\times10^{-12}\,C\,V^{-1}\,m^{-1}$). In the present study, samples' thicknesses were evaluated with a Mitutoyo micrometer, model M110-25. The sample's thicknesses were about $12.0\pm0.5\,\mu m$.

The electrical properties of the ST–GO samples, before and after photochemical reduction, were determined by current *versus* potential curves obtained with the HP 4156A Semiconductor Parameter Analyzer. The ST–GO and ST–RGO films ($1.0\times2.5\,cm^2$) were coated with four equidistant silver epoxy contacts (MG Chemicals 8331 Conductive Epoxy Adhesive) through which gold microprobes were connected to perform electrical measurements. A fixed current was applied through the two external contacts, and the voltage drop across the two inner contacts was thus, measured.

3. Results and discussion

3.1. Structure and morphology of ST-GO nanocomposite films

Fig. 1 provides UV–vis absorption spectra along with digital snapshots of ST–GO nanocomposites with different amounts of GO. Similarly to the GO aqueous suspension (not shown), the spectra of nanocomposites (Fig. 1a) exhibit two maxima absorption peaks located at 230 nm and 300 nm, which are ascribed to the $\pi\longrightarrow\pi^*$ transition in aromatic C=C bonds and the $n\longrightarrow\pi^*$ transition in carbonyl groups, respectively (Li, Muller, Gilje, Kaner, & Wallace, 2008; Guardia et al., 2012). The nanocomposites also display the same brownish color of GO suspension, and they become darker as more GO is incorporated (Fig. 1b). In addition, the transparency as estimated by the film transmittance (400–700 nm) of nanocomposites drastically reduces with incorporation of GO. For example, the ST–GO-0.10 sample has a transmittance of 75%, which then reduces to 35% in the ST–GO-0.25, and then to 20% (ST–GO-0.50) and less than 20% for the ST–GO-0.75.

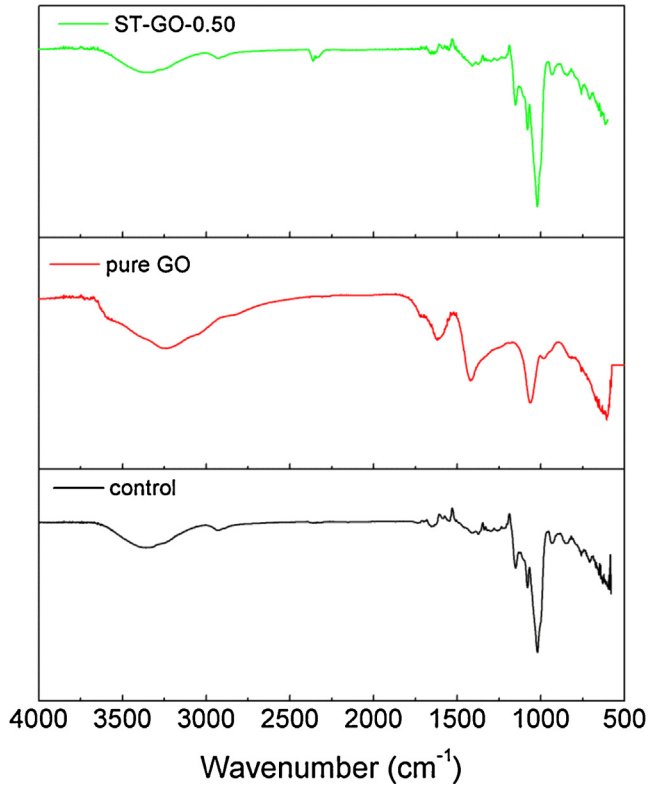

Fig. 2. ATR-FTIR spectra of control (black), pure GO (red), and ST–GO-0.50 nanocomposite (green) samples. (For interpretation of the references to colour in this figure legend, the reader is referred to the web version of this article.)

The ATR-FTIR spectra of control, pure GO and ST–GO-0.50 nanocomposite are presented in Fig. 2. The band referred to the stretching of O—H bond is clearly seen in the three samples. While in the control and in the ST–GO-0.50 nanocomposite, this band peaks at 3360 cm^{-1}, in pure GO the same band is more asymmetric and exhibits a maximum at shorter wavenumber (3235 cm^{-1}). In the range below 2000 cm^{-1}, the fingerprints of starch component are readily recognized in both the control and the ST–GO-0.50 nanocomposite. In fact, the ST–GO-0.50 nanocomposite spectrum (in green) is almost indistinguishable from the control (in black) and shows none of the bands seen in the GO spectrum (in red). The main vibration modes in the control sample (in black) have been ascribed in accordance to literature (Flores-Morales, Jiménez-Estrada & Mora-Escobedo, 2012) as follows: C=O stretching of the acetylated groups (1742 cm^{-1}); O—H bending (1652 cm^{-1}); C—O stretching (1154 cm^{-1}); C—O—H stretching (1082 cm^{-1}); C—O—H bending (1022 cm^{-1}); and C—O—C bending of α-1,4-glycosidic bond (998 cm^{-1}). In the spectrum of the ST–GO-0.50 nanocomposite (in green), most of bands have been systematically shifted to shorter wavenumbers. This trend suggests the interaction of starch and GO via hydrogen bonding. The assignments for bands in the ST–GO-0.50 sample have been made as follows: C=O stretching of the acetylated groups (1742 cm^{-1}); O—H bending (1640 cm^{-1}); C—O stretching (1150 cm^{-1}); C—O—H stretching (1078 cm^{-1}); C—O—H bending (1022 cm^{-1}); and C—O—C bending of α-1,4-glycosidic bond (997 cm^{-1}). The greatest shift has been observed for the O—H bending, which is about 12 cm^{-1}. The spectrum of pure GO displays the oxygen-bearing functionalities that have been introduced after graphite oxidation. In accordance to literature (Hontoria-Lucas, Lopez-Peinado, Lopez-Gonzalez, Rojas-Cervantes,

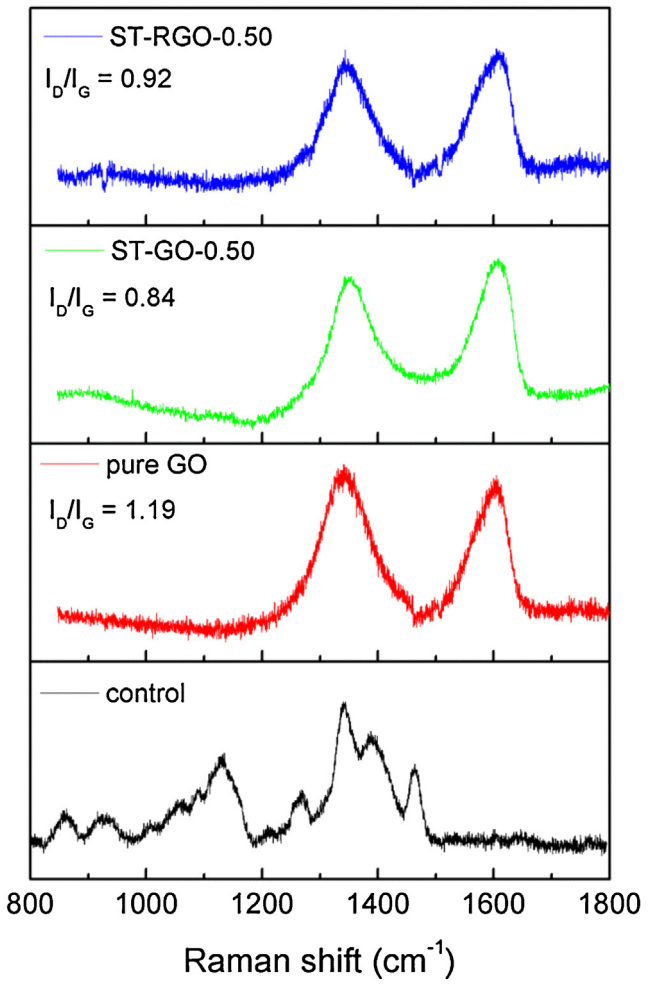

Fig. 3. Raman spectra of control (starch + PVA, in black), pure GO (in red), ST–GO-0.50 nanocomposite (in green), and ST–RGO-0.50 nanocomposite (in blue). The spectrum in blue refers to the one obtained after the ST–GO-0.50 has been submitted to UV exposition for 160 min, as described in Section 2.4. (For interpretation of the references to colour in this figure legend, the reader is referred to the web version of this article.)

& Martin-Aranda, 1995) the assignments for such bands have been made as follows: C═O stretching (1714 cm^{-1}); C═C stretching (1612 cm^{-1}); C—O—H bending (1417 cm^{-1}); C—O—C stretching (1060 cm^{-1}); and ═C—H bending (980 cm^{-1}). The spectra of other ST–GO nanocomposites have showed similar features and are not presented.

Raman spectra of control, pure GO, and ST–GO-0.50 nanocomposite samples are shown in Fig. 3. As a general observation, GO bands screen any other bands from the starch + PVA matrix. The same trend has been observed for all other ST–GO compositions, and for that reason, their corresponding spectra are not shown. This effect is ascribed to the use of 514 nm excitation that matches better GO vibrations than starch ones. The spectrum of the control sample features the C—O and C—C stretching as well as the C—O—C deformation modes typical of the glycosidic bonds in starch. In accordance to literature (Almeida et al., 2010; Rodríguez-González et al., 2012), the main vibrations (wavenumbers assigned in the spectrum) have been tentatively ascribed as follows: bending of C—C—H and C—O—C bonds (858 and 925 cm^{-1}); stretching of C—O and C—C bonds (1129 and 1209 cm^{-1}); bending of C—C—H, O—C—H and C—O—H bonds (1266 cm^{-1}); stretching of C—O and bending of C—O—H bonds (1340 cm^{-1}); bending of C—O—H bond (1387 cm^{-1}), and bending of C—H and C—O—H bonds (1462 cm^{-1}). The distinct bands at 925 and 858 cm^{-1} are referred to vibrations originated from α-1,4 glycosidic linkages and provide a fingerprint for the amylose component of starch. The spectrum of pure GO (in red) displays two intense bands at 1340 and 1600 cm^{-1}. The first, the D-band, corresponds to the breathing mode of k-point phonons of A_{1g} symmetry while the second one, the G-band, corresponds to the first-order scattering of the E_{2g} phonon of sp^2 carbons. Both bands are regarded to the graphene structure according to literature (Saito, Hofmann, Dresselhaus, Jorio, & MS, 2011). The spectrum of the ST–GO-0.50 nanocomposite (in green) exclusively features bands regarding GO. This screening effect has been discussed above. The relative Raman D/G intensity ratio (I_D/I_G) is inversely proportional to the average size of the sp^2 domains (Saito et al., 2011). In the case of our pure GO, I_D/I_G = 1.19, while for the ST–GO-0.50 nanocomposite, I_D/I_G = 0.84. The slight decrease of I_D/I_G when going from pure GO to ST–GO-0.50 nanocomposite has no explanation so far. As to other nanocomposites compositions, we have found no correlation between I_D/I_G and GO content, which has remained almost constant: 0.86 (ST–GO-0.10); 0.81 (ST–GO-0.25); 0.84 (ST–GO-0.50); and 0.87 (ST–GO-0.75). After the photochemical treatment, which will be discussed in detail at Section 3.3, the I_D/I_G ratio in the nanocomposite sample with 0.50 wt% of GO and now labeled ST–RGO-0.50, underwent a slight increase to about 0.92. This increase corresponds to reduction reactions of the GO phase, as already proposed by Stankovich and coworkers (Stankovich et al., 2007).

Fig. 4 presents SEM images of the surface (top) and cross section (bottom) of nanocomposites. While the surface of all samples, including that of the control, is relatively flat and smooth, the cross section after fracture is more irregular on the nanocomposites with GO. This is because GO is well dispersed and strongly adhered to the starch–PVA matrix.

3.2. Thermal properties

Fig. 5 shows TG curves of the control and GO-containing nanocomposites. In Fig. 5a, the thermal behavior of the ST–GO-0.50 nanocomposite is compared to that of the control and pure GO. For pure GO (curve in black), one observes the decomposition at 200 °C associated to a mass loss of about 60%. This event has been associated to the dehydration of oxygenated groups accompanied by the partial reestablishment of the pi-conjugated system (Silva et al., 2010). The latter event maintains the partially reduced GO stable so that the residue after reaching 600 °C is about 30%, which is greater than that left after decomposition of pure starch or the ST–GO-0.50 nanocomposite. As to pure starch, the TG curve (in blue) presents two main thermal events, the first one at ~100 °C that corresponds to the water elimination and a second event, at 300 °C, which is regarded to elimination of polyhydroxyl groups and starch depolymerization (Schlemmer, Sales, & Resck, 2010; Schlemmer & Sales, 2010). At 600 °C, almost all starch is decomposed. The nanocomposites's TG curve (in red) displays the elimination of water as well as the decomposition of starch. However, the residual mass at 600 °C is slightly greater than the control, most likely due to the residual, more stable GO.

In Fig. 5b, TG curves of ST–GO nanocomposites are presented for evaluating the effect of GO on their thermal stability. As one notes, as more GO is incorporated, the onset for the main decomposition event occurs at lower temperature whereas the residual mass at 600–°C increases. The lowering on temperature of the main decomposition is attributed to the intercalation of GO sheets in between starch chains. This certainly reduces the intermolecular forces in starch as well as provides more oxygen reactive species that contribute for the starch decomposition. This result has been shared by other investigators working on similar systems (Ma, Chang, Zheng, & Ma, 2013; He et al., 2013; Li et al., 2011). This

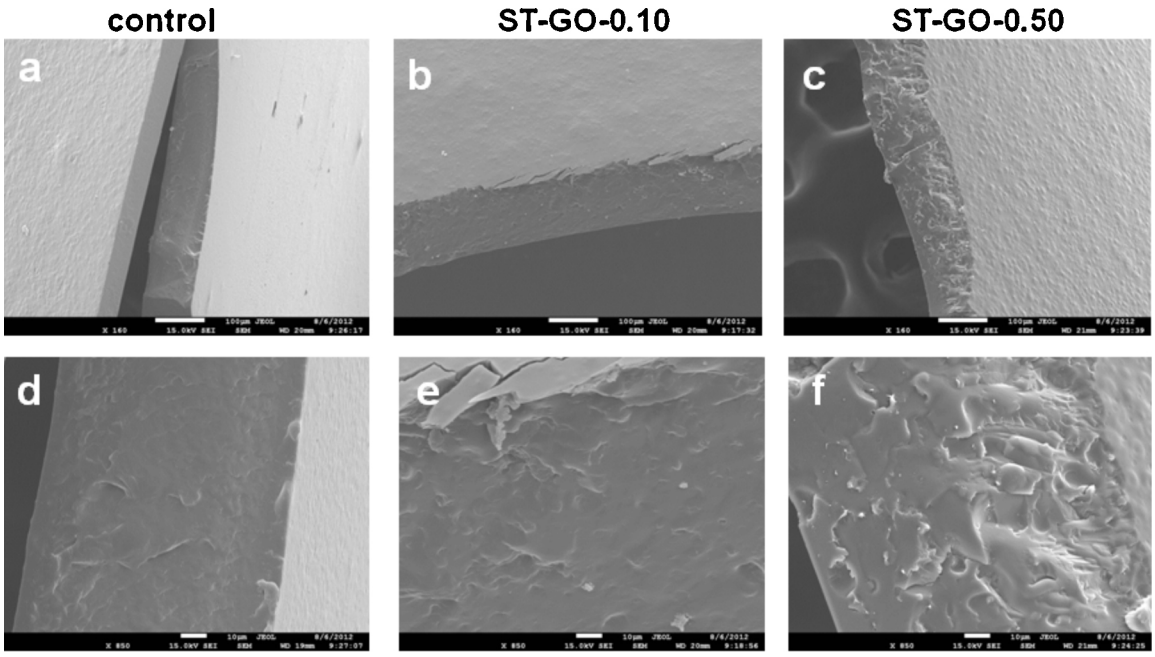

Fig. 4. SEM images of surface (top images; scale bar: 100 μm) and cross section (bottom images; scale bar: 10 μm) of nanocomposites: control (a) and (d); ST–GO-0.10 (b) and (e); and ST–GO-0.50 (c) and (f).

Table 1
Thermal properties of control and ST–GO nanocomposites.

Sample	Enthalpy ($J g^{-1}$)	Thermal diffusivity ($\times 10^{-4}$ cm^2 s^{-1})	
		Before reduction	After reduction
Control	465.11	1.86	–
ST–GO-0.10	491.15	1.92	7.1
ST–GO-0.25	196.27	3.08	8.3
ST–GO-0.50	102.12	3.59	11.5
ST–GO-0.75	84.36	7.19	17.5

hypothesis is corroborated further by data collected in Table 1 (second column) that shows that more the GO is introduced the lower is the enthalpy for the water elimination. This observation along with ATR-FTIR data (Fig. 2) allows one to conclude that GO sheets replace water molecules in the nanocomposite while establishing hydrogen bonds with starch and PVA chains. Additionally, Table 1 (third column) collects thermal diffusivities measured accross the samples. The data show that samples containing GO are better thermal conductors than the control sample. This improvement has been ascribed to the few graphene domains remaining in GO after graphite oxidation. The outstanding thermal conduction in deffect free graphene is ascribed to the in-plane scattering of phonons (in the diffusion limit regime) (Pop, Varshney, & Roy, 2012).

3.3. Photochemical reduction of ST–GO nanocomposites

The network structure of GO sheets is highly attractive and potentialy promising for the improvement of mechanical properties of biopolymers such as starch. However, its optoelectronic properties are still very poor as the pi-conjugated system is partially disrupted after the graphite oxidation. Thus, the restoring of such conjugated structure is mandatory for the attainment of electrical conducting composites. Generally, reductive chemicals such as hydrazine and sodium borohydride, have been successfully employed for this task even though they involve severe health and environmental concerns. In this sense, milder reduction approaches have been pursued and photochemical procedures have called special attention. The photochemical reduction of GO to RGO by UV light has been made possible because GO sheets strongly absorb energy at this wavelength and subsequent relaxation processes could trigger a local heating of the sheets that favors their deoxygenation (Kumar et al., 2012; Guardia et al., 2012; Fabbri et al., 2012). Such a reduction method would provide the means by which one can easily produce RGO with relatively less impurity.

Considering those aspects, we have exposed the ST–GO-0.50 nanocomposite to an UV light source (354 nm) and followed by UV–vis spectroscopy, the structural changes caused by the irradiation (see Section 2.3). According to Fig. 6, the ratio of UV absorbances at 250 and 300 nm, which are ascribed to $n \longrightarrow \pi^*$ (C=O) and $\pi \longrightarrow \pi^*$ (C=C) transitions, respectively, decreases with the exposure time. Moreover, the snapshopts in the inset show that the nanocomposite, initially brown, have become deeply dark at the end of treatment (after 160 min of exposure). A control experiment performed in the same conditions with the control film has not showed any darkening effect of the starch matrix.

To confirm the effectiveness of the proposed photochemical reduction method, we have carried out Raman spectroscopy as well as measured the thermal diffusivity and electrical properties of nanocomposites. As displayed by Fig. 3, the I_D/I_G ratio increases from 0.84 (ST–GO-0.50, in green) to 0.91 (ST–RGO-0.50, in blue) after the photochemical treatment. It is known that the I_D/I_G ratio is inversely proportional to the average size of sp^2 domains (Tuinstra & Koenig, 1970). Thus, the increase that has been observed herein suggests that new graphitic domains have been created and that they are smaller in size to the ones present in GO before reduction, but more numerous. In summary, part of the pi-conjugated system is recovered, which is consistent with the GO $\longrightarrow$ RGO reduction. The photochemical treatment has increased thermal diffusivities one order of magnitude, as quoted in Table 1 (fourth column), as RGO is a better thermal conductor than GO.

The reduction of GO phase within the nanocomposites was also probed by electrical measurements. Fig. 7 displays current *versus* voltage curves for the ST–GO-0.50 nanocomposite before and after the photochemical treatment. For the same voltage range, the current measured within the nanocomposite has increased two orders of magnitude after the photochemical treatment. The different colors refer to curves aquired through different contact pairs on the

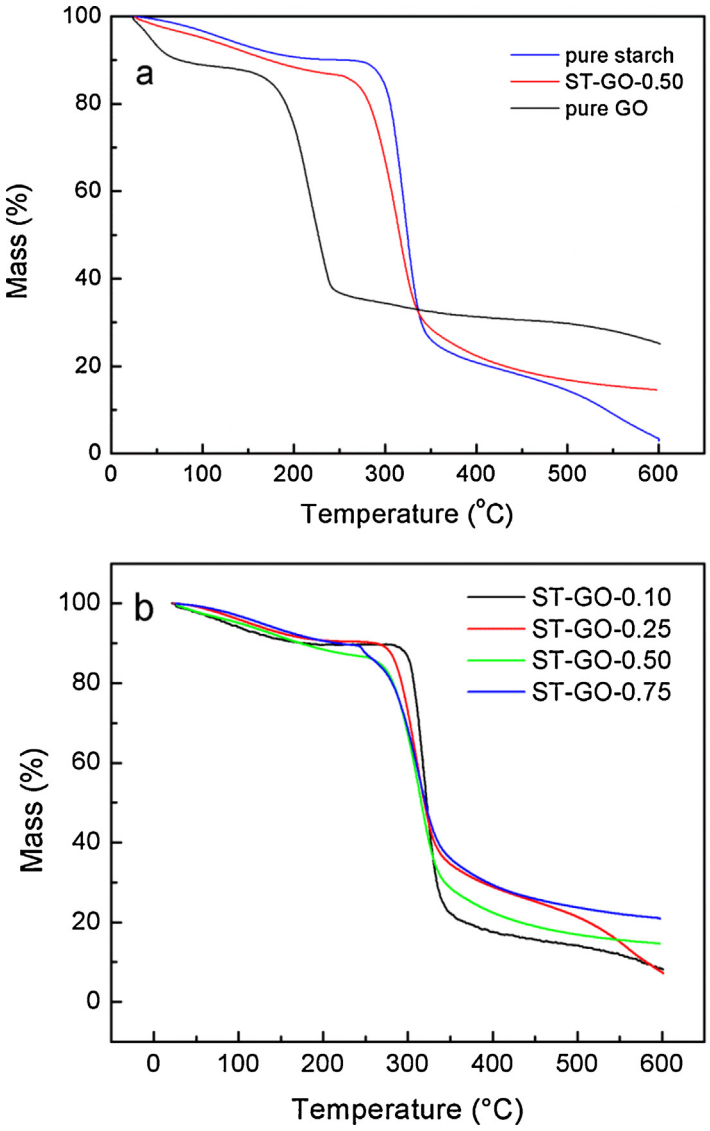

Fig. 5. TG curves of (a) pure starch, pure GO, and ST–GO-0.50 nanocomposite and (b) ST–GO nanocomposites with different loadings of GO, as indicated. (For interpretation of the references to colour in this figure legend, the reader is referred to the web version of this article.)

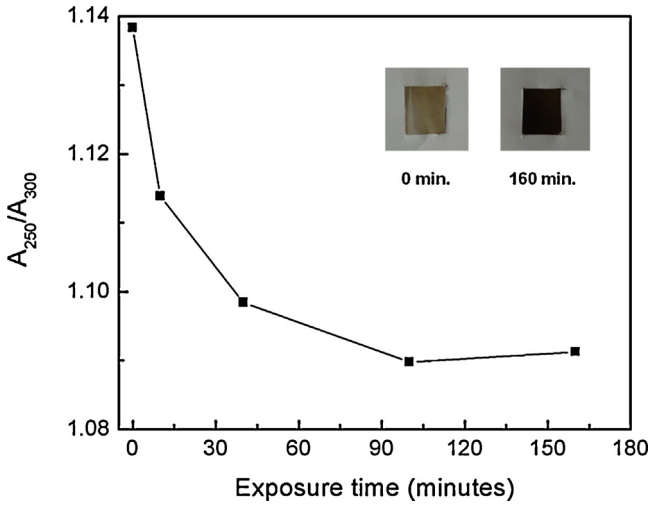

Fig. 6. Monitoring of absorbance ratios (A_{250}/A_{300}) of the ST–GO-0.50 nanocomposite as a function of the exposure time to UV light (254 nm). Inset: snapshots of nanocomposite sample at the beggining (0 min) and after 160 min of exposure.

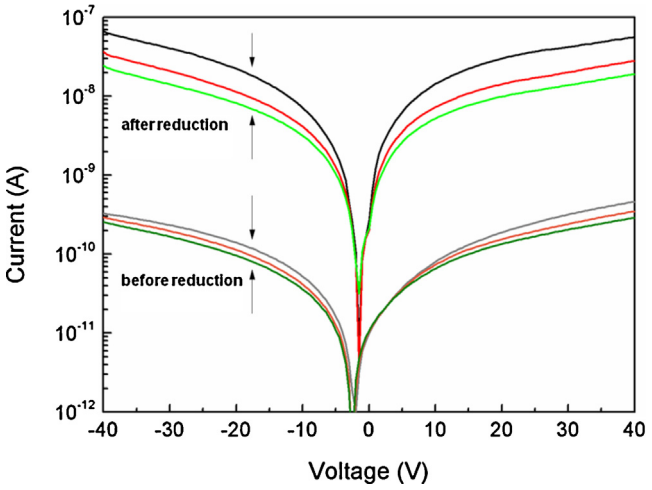

Fig. 7. Current *versus* voltage curves for ST–GO-0.50 nanocomposite before and after photochemical reduction. The different colors refer to curves aquired between two different pairs of contacts on the sample. (For interpretation of the references to colour in this figure legend, the reader is referred to the web version of this article.)

sample. It is possible to note that data drift is very low when measurement contacts are changed because samples and contacts are quite uniform. The overpotential seen for the sample before reduction (bottom curves) has been credited to its highly insulating behavior. Based on these results, one can conclude that the photochemical treatment is sufficient to reduce GO to RGO and to improve the thermal and electrical properties of the ST–GO nanocomposite.

4. Conclusions

Starch–graphene oxide nanocomposites (ST–GO) exhibit better thermal and electrical properties when the amount of the GO phase is increased and properly converted to reduced graphene oxide (RGO), respectively. Because water molecules are readily replaced by GO sheets, the latter interact with the ST matrix through hydrogen bonds, the enthalpy for water release from the nanocomposites become significant lower as more GO is introduced. However, GO sheets also reduce the interaction between ST domains and induce their degradation at lower temperatures. A reagentless photochemical method for conversion of the GO phase into RGO increases the thermal diffusivity and lowers the electrical resistance of nanocomposites to about one and two orders of magnitude, respectively. Raman and UV–vis absorption spectroscopies provide strong evidence for the partial restoring of the pi-conjugated system after the photochemical treatment. In summary, the ST–GO nanocomposites and the photochemical approaches described herein enable one for the production of low cost and environmentally friendly nanomaterials with potential thermal and electrical properties.

Acknowledgements

The financial support of Brazilian agencies CNPq (process # 308038/2012-6), CAPES, and Finatec is greatfully acknowledged. The authors also wish to thank Dr. Roberto Cavallari (PSI-EPUSP) for the electrical characterizations.

References

Almeida, M. R., Alves, R. S., Nascimbem, L. B., Stephani, R., Poppi, R. J., & Oliveira, L. F. (2010). Determination of amylose content in starch using Raman spectroscopy and multivariate calibration analysis. *Analytical Bioanalytical Chemistry*, *397*, 2693–26701.

Chaharmahali, M., Hamzeh, Y., Ebrahimi, G., Ashori, A., & Ghasemi, I. (2014). Effects of nano-graphene on the physico-mechanical properties of bagasse/polypropylene composites. *Polymer Bulletin*, *71*, 337–349.

Darder, M., Aranda, P., & Ruiz-Hitzky, E. (2007). Bionanocomposites: A new concept of ecological, bioinspired, and functional hybrid materials. *Advanced Materials*, *19*, 1309–1319.

Fabbri, P., Valentini, L., Bon, S. B., Foix, D., Pasquali, L., Montecchi, M., & Sangermano, M. (2012). In-situ graphene oxide reduction during UV-photopolymerization of graphene oxide/acrylic resins mixtures. *Polymer*, *53*, 6039–6044.

Flores-Morales, A., Jiménez-Estrada, M., & Mora-Escobedo, R. (2012). Determination of the structural changes by FTIR, Raman, and CP/MAS ^{13}C NMR spectroscopy on retrograded starch of maize tortillas. *Carbohydrate Polymers*, *87*, 61–68.

Guardia, L., Villar-Rodil, S., Paredes, J. I., Rozada, R., Martinez-Alonso, A., & Tascon, J. M. D. (2012). UV light exposure of aqueous graphene oxide suspensions to promote their direct reduction, formation of graphene–metal nanoparticle hybrids and dye degradation. *Carbon*, *50*, 1014–1024.

He, Y., Wang, X., Wu, D., Gong, Q., Qiu, H., Liu, Y., Wu, T., Ma, J., & Gao, J. (2013). Biodegradable amylose films reinforced by graphene oxide and polyvinyl alcohol. *Materials Chemistry and Physics*, *142*, 1–11.

Hontoria-Lucas, C., Lopez-Peinado, A. J., Lopez-Gonzalez, J. D., Rojas-Cervantes, M. L., & Martin-Aranda, R. M. (1995). Study of oxygen-containing groups in a series of graphite oxides: Physical and chemical characterization. *Carbon*, *33*, 1585–1592.

Jaber-Ansari, L., & Hersam, M. C. (2012). Solution-processed graphene materials and composites. *MRS Bulletin*, *37*, 1167–1175.

Kumar, P., Das, B., Chitara, B., Subrahmanyam, K. S., Gopalakrishnan, K., Krupanidhi, S. B., & Rao, C. N. R. (2012). Novel radiation-induced properties of graphene and related materials. *Macromolecular Chemistry and Physics*, *213*, 1146–1163.

Li, D., Muller, M. B., Gilje, S., Kaner, R. B., & Wallace, G. G. (2008). Processable aqueous dispersions of graphene nanosheets. *Nature Nanotechnology*, *3*, 101–105.

Li, R., Liu, C., & Ma, J. (2011). Studies on the properties of graphene oxide reinforced starch biocomposites. *Carbohydrate Polymers*, *84*, 631–637.

Ma, J., Liu, C., Li, R., & Wang, J. (2012). Properties and structural characterization of oxide starch/chitosan/graphene oxide biodegradable nanocomposites. *Journal of Applied Polymer Science*, *123*, 2933–2944.

Ma, T., Chang, P. R., Zheng, P., & Ma, X. (2013). The composites based on plasticized starch and graphene oxide/reduced graphene oxide. *Carbohydrate Polymers*, *94*, 63–70.

Mandelis, A., & Zver, M. M. (1985). Theory of photopyroelectric spectroscopy of solids. *Journal of Applied Physics*, *57*, 4421–4430.

Paraginski, R. T., Vanier, N. L., Moomand, K., de Oliveira, M., Zavareze, E. R., Silva, R. M., Ferreira, C. D., & Elias, M. C. (2014). Characteristics of starch isolated from maize as a function of grain storage temperature. *Carbohydrate Polymers*, *102*, 88–94.

Pop, E., Varshney, V., & Roy, A. K. (2012). Thermal properties of graphene: Fundamentals and applications. *MRS Bulletin*, *37*, 1273–1281.

Rodríguez-González, C., Martínez-Hernández, A. L., Castaño, V. M., Kharissova, O. V., Ruoff, R. S., & Velasco-Santos, C. (2012). Polysaccharide nanocomposites reinforced with graphene oxide and keratin-grafted graphene oxide. *Industrial & Engineering Chemistry Research*, *51*, 3619–3629.

Saito, R., Hofmann, M., Dresselhaus, G., Jorio, A., & Dresselhaus, M. S. (2011). Raman spectroscopy of graphene and carbon nanotubes. *Advances on Physics*, *60*, 413–550.

Schlemmer, D., Sales, M. J. A., & Resck, I. S. (2010). Preparação, caracterização e degradação de blendas PS/TPS usando glicerol e óleo de buriti como plastificantes. *Polímeros: Ciência e Tecnologia*, *20*, 6–13.

Schlemmer, D., & Sales, M. J. A. (2010). Thermoplastic starch films with vegetable oils of Brazilian Cerrado. *Journal of Thermal Analysis and Calorimetry*, *99*, 675–679.

Sheshmani, S., Ashori, A., & Fashapoyeh, M. A. (2013). Wood plastic composite using graphene nanoplatelets. *International Journal of Biological Macromolecules*, *58*, 1–6.

Silva, M. F. P. H., Costa, C. J. F., Triboni, E. R., Politi, M. J., & Isolani, P. C. (2010). Synthesis and characterization of CeO_2–graphene composite. *Journal of Thermal Analysis and Calorimetry*, *102*, 907–913.

Staudenmaier, L. (1898). Verfahren zur Darstellung der Graphitsäure. *Berichte der Deutschen Chemischen Gesellschaft*, *31*, 1481–1487.

Stankovich, S., Dikin, D. A., Piner, R. D., Kohlhaas, K. A., Kleinhammes, A., Jia, Y., Wu, Y., Nguyen, S. B. T., & Ruoff, R. S. (2007). Synthesis of graphene-based nanosheets via chemical reduction of exfoliated graphite oxide. *Carbon*, *45*, 1558–1565.

Tang, X. Z., Kumar, P., Alavi, S., & Sandeep, K. P. (2012). Recent advances in biopolymers and biopolymer-based nanocomposites for food packaging materials. *Critical Review in Food Science and Nutrition*, *52*, 426–442.

Tuinstra, F., & Koenig, J. L. (1970). Raman spectrum of graphite. *Journal of Chemical Physics*, *53*, 1126–1130.

Tung, V. C., Allen, M. J., Yang, Y., & Kaner, R. B. (2009). High-throughput solution processing of large-scale graphene. *Nature Nanotechnology*, *4*, 25–29.

Zhu, Y., Murali, S., Cai, W., Li, X., Suk, J. W., Potts, J. R., & Ruoff, R. S. (2010). Graphene and graphene oxide: Synthesis, properties, and applications. *Advanced Materials*, *22*, 3906–3924.